J. Fluid Mech. (2025), *vol.* 1023, A48, doi:10.1017/jfm.2025.10844

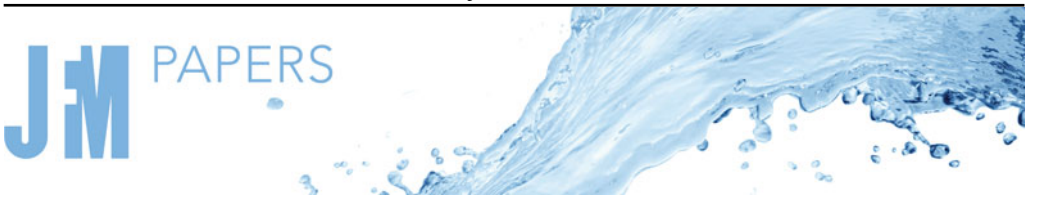

Turbulent transport for wall-shear-stress fluctuations

Myoungkyu Lee[1] **and Yongyun Hwang**[2]

[1]Department of Mechanical and Aerospace Engineering, University of Houston, Houston, TX, USA

[2]Department of Aeronautics, Imperial College London, London SW7 2AZ, UK

Corresponding author: Myoungkyu Lee, leemk@uh.edu

(Received 15 February 2025; revised 14 October 2025; accepted 15 October 2025)

Statistical structure and the underlying energy budget of wall-shear-stress fluctuations are studied in both Poiseuille and Couette flows with emphasis on its streamwise component. Using a dimensional analysis and direct numerical simulation data, it is shown that the spectra of streamwise wall dissipation for $\lambda \lesssim 1000\delta_\nu$ are asymptotically invariant with the Reynolds number (Re), whereas those for $\lambda \gtrsim \delta$ decay with Re (here, λ is a nominal wall-parallel wavelength, and δ_ν and δ are the viscous inner and outer length scales, respectively). The wall dissipation increases with Re due to the increasing contribution of the spectra at $1000\delta_\nu \lesssim \lambda \lesssim \delta$. The subsequent analysis of the energy budget shows that the near-wall motions associated with these wall-dissipation spectra are driven mainly by turbulent transport and are 'inactive' in the sense that they contain very little Reynolds shear stress (or turbulence production). As such, turbulent-transport spectra near the wall are also found to share the same Re-scaling behaviour with wall dissipation, and this is observed in the spectra of both the wall-normal and inter-scale turbulent transports. The turbulent transport underpinning the increase of wall dissipation with Re is characterised by energy fluxes towards the wall, together with inverse energy transfer from small to large length scales along the wall-parallel directions.

Key words: turbulence theory, turbulent boundary layers, turbulent flows

1. Introduction

The precise understanding of how fluctuation energy is transported and dissipated through nonlinear interactions between flow structures across a wide range of scales is an outstanding challenge in the studies of turbulence. In wall-bounded turbulence, the large

© The Author(s), 2025. Published by Cambridge University Press. This is an Open Access article, distributed under the terms of the Creative Commons Attribution-NonCommercial-ShareAlike licence (https://creativecommons.org/licenses/by-nc-sa/4.0/), which permits non-commercial re-use, distribution, and reproduction in any medium, provided the same Creative Commons licence is used to distribute the re-used or adapted article and the original article is properly cited. The written permission of Cambridge University Press must be obtained prior to any commercial use.

https://doi.org/10.1017/jfm.2025.10844 Published online by Cambridge University Press

separation between the inner and outer length scales is a distinctive feature at high Reynolds numbers (Re), and interactions across these scales are crucially involved in the dynamical and statistical processes of the flow (e.g. Cho, Hwang & Choi 2018; Lee & Moser 2019). In particular, above the near-wall region, there exist a large number of hierarchically organised energy-containing motions, the size of which varies from their distance from the wall to the outer length scale (Townsend 1976; Marusic & Monty 2019). With increasing Re, the overall impact of these motions becomes more pronounced. It also manifests as the increased peak values in the streamwise velocity variances and the enhanced dissipation of turbulent kinetic energy (e.g. de Graaff *et al.* 2000; Marusic & Kunkel 2003; Hwang 2024; Pirozzoli 2024), although there is a different view proposed recently (see e.g. Chen & Sreenivasan 2021, 2022; Monkewitz 2022). Of particular interest in this study is the fluctuation in wall shear stress, a central property of near-wall turbulence relevant to many engineering applications.

In his early study, Townsend (1976) speculated that shear stress on the wall contains a slowly fluctuating part, linked with the 'inactive' part of energy-containing motions in the logarithmic and outer regions. These inactive motions are defined to be with little Reynolds shear stress due to the boundary condition on the wall, which prevents the formation of the wall-normal velocity. In the last decade, there has been growing evidence on the presence of such inactive motions in the vicinity of the wall (e.g. Hwang 2015; Lee & Moser 2015; Hwang 2016; Deshpande, Monty & Marusic 2020). Strong correlations have also been consistently observed between the large-scale components of velocity fields across the entire wall-normal locations (e.g. Hoyas & Jiménez 2006; Hutchins & Marusic 2007; Mathis, Hutchins & Marusic 2009), indicating that they may be the consequence of a transfer of energy from the outer flow to the near-wall flow (Lee & Moser 2019; Deshpande *et al.* 2024; Yin, Hwang & Vassilicos 2024). More recent research has used observed fluctuations in wall shear stress to propose a unified scaling for velocity variance and to extrapolate velocity fields further from the wall (Smits *et al.* 2021).

Despite the recent progress mentioned, it remains to be understood how these inactive motions near the wall statistically scale and are dynamically formed, especially at high Re. Given their origin, the size of inactive motions (say l) is supposed to be much larger than that of energy-containing motions in the near-wall region, such as streaks (Kline *et al.* 1967) and quasi-streamwise vortices (Jeong *et al.* 1997), i.e. $l \gg \delta_\nu (\equiv \nu/u_\tau$, where ν and u_τ are the kinematic viscosity and friction velocity, respectively). Furthermore, they do not carry wall-normal velocity fluctuations, indicating that the related turbulence production must be negligible. Therefore, if pressure transport at such large length scales is assumed to be negligible (Lee & Moser 2019, see also § 3.2), the inactive motions would be driven primarily by turbulent transport near the wall and subsequently contribute to dissipation of the turbulence on the wall. We note that the rate of streamwise dissipation at the wall, ϵ_w, relates directly to the streamwise wall-shear-stress fluctuation, τ_w':

$$\epsilon_w = -\nu \langle (\tau_w'/\mu)^2 \rangle, \tag{1.1}$$

where μ is fluid viscosity and $\langle \cdot \rangle$ is an average in time and in homogeneous directions.

The shear-stress fluctuations (or dissipation) on the wall are also related to near-wall velocity fluctuations. In the region close to the wall, the streamwise turbulent kinetic energy (TKE) is approximated as

$$\langle u'u' \rangle^+ = \epsilon_w^+ (y^+)^2 + O((y^+)^3), \tag{1.2}$$

where u' is the streamwise velocity fluctuation and the superscript $(\cdot)^+$ denotes normalisation with u_τ and ν. Figure 1 shows the two-dimensional spectral densities

https://doi.org/10.1017/jfm.2025.10844 Published online by Cambridge University Press

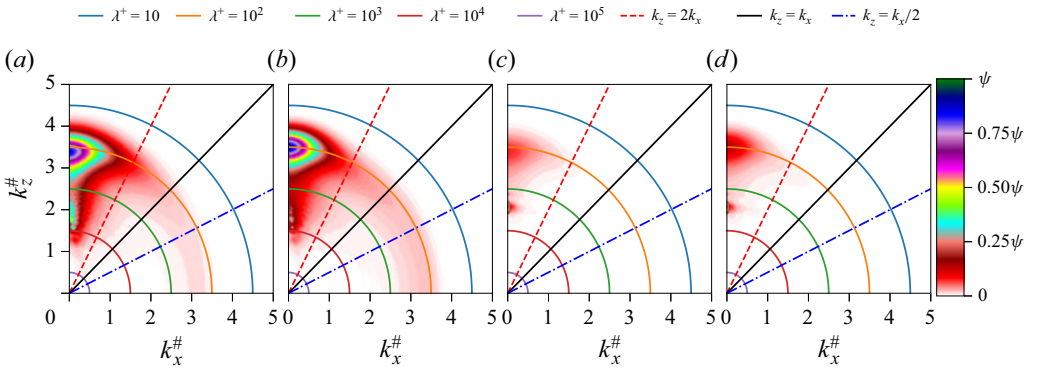

Figure 1. Two-dimensional spectral densities in polar-log coordinates of u'^2 and ϵ_w, $k_{ref} = 1/(50\,000\delta_v)$: (*a*) $E^\#_{u'^2}$ at $y^+ = 15$, $Re_\tau = 5200$, Poiseuille, $\psi = 13$ (*b*) $E^\#_{\epsilon_w}$, $Re_\tau = 5200$, Poiseuille, $\psi = 0.67$ (*c*) $E^\#_{u'^2}$ at $y^+ = 15$, $Re_\tau = 500$, Couette, $\psi = 45$ (*d*) $E^\#_{\epsilon_w}$, $Re_\tau = 500$, Couette, $\psi = 4.4$. Here, the contour levels are suitably chosen to reveal the similarities between the spectral densities of u'^2 and ϵ_w. https://www.cambridge.org/S0022112025108446/JFM-Notebooks/files/figure01/Fig01.ipynb. See § 2 for the mathematical definition of spectral densities in polar-log coordinates.

of u'^2 at $y^+ = 15$ and ϵ_w^+ in the polar-log coordinates (see § 2 for their definition) for plane Poiseuille flows, driven by a pressure gradient, and Couette flows, driven by boundary movement. Both spectral densities share strong structural similarities, and their importance for Poiseuille flows has been discussed extensively in Smits *et al.* (2021). Recently, in relation to (1.2), Chen & Sreenivasan (2021) proposed that the wall dissipation is possibly bounded in the limit of $Re \to \infty$ and the influence of near-wall bursting on wall dissipation would play a key role in understanding how the peak streamwise turbulence intensity in the near-wall region would scale with Re. From this perspective, a precise understanding of the nature of turbulent transport in the near-wall region would illuminate the physical process that underpins the scaling of the near-wall turbulence intensity with Re (Chen & Sreenivasan 2021; Hwang 2024; Jimenez 2024; Pirozzoli 2024)

The objective of this study is to explore the statistical structure and scaling of turbulent transport associated with wall-shear-stress fluctuations. The primary focus is given to the streamwise wall-shear-stress fluctuations. We consider two different forms of wall-bounded turbulence across various Re: Poiseuille and Couette flows chosen for their different large-scale behaviours. In Couette flows, the large-scale structures in the outer region are very energetic due to the non-zero turbulence production and mean shear at the channel centre. It was observed that a simulation domain with a streamwise length of $L_x = 100\pi\delta$ (δ is half the height of the channel) did not adequately encompass these structures present in Couette flows at $Re_\tau = 500$ where Re_τ is the friction Reynolds number (Lee & Moser 2018): see also Hoyas & Oberlack (2024) for this issue at higher Re. In contrast, in Poiseuille flows, the production at the channel centre is zero due to vanishing mean shear and Reynolds shear stress at the location. Therefore, the large-scale structures tend to be significantly less energetic than those in Couette flows.

This paper is organised as follows. In § 2, we briefly introduce the datasets to be used and the statistical analysis tool (two-dimensional spectra of the energy budget in the polar-log coordinate). The nature of wall-dissipation spectra and the related turbulent-transport spectra are studied in § 3 with their scaling behaviour. A summary, a discussion and implications of the results are finally presented in § 4.

https://doi.org/10.1017/jfm.2025.10844 Published online by Cambridge University Press

2. Streamwise spectral energy and its budget

The present study uses the results of direct numerical simulations (DNS) of turbulent flows (Lee & Moser 2015, 2018). These results are produced using the simulation software from Lee, Malaya & Moser (2013), which employs Fourier-spectral methods to calculate derivatives in the streamwise (x) and spanwise (z) directions, along with the seventh-order basis spline methods for derivatives in the wall-normal (y) direction: for detailed information on the simulation methodology, the reader may refer to previous studies (Lee *et al.* 2013; Lee & Moser 2015, 2018). Throughout this study, u, v and w indicate the velocity component in the streamwise, wall-normal and spanwise directions, respectively, and the prime denotes the fluctuations. Also, p denotes the pressure.

To understand the behaviour in the streamwise wall dissipation and its origin, we consider the following spectral energy balance:

$$\frac{\partial E_{u'^2}}{\partial t} = E^P_{u'^2} + E^{\Pi}_{u'^2} + E^T_{u'^2} + E^D_{u'^2} - E^{\epsilon}_{u'^2} = 0, \quad \forall (k_x, y, k_z) \tag{2.1a}$$

where

$$E_{u'^2} = \langle \hat{u}' \hat{u}'^* \rangle_{\mathcal{T}}, \tag{2.1b}$$

$$E^P_{u'^2} = -\langle \hat{u}' \hat{v}'^* + \hat{u}'^* \hat{v}' \rangle_{\mathcal{T}} \frac{\partial \langle u \rangle}{\partial y}, \tag{2.1c}$$

$$E^{\Pi}_{u'^2} = -\left\langle \hat{u}' \widehat{\frac{\partial p'}{\partial x}}^* + \hat{u}'^* \widehat{\frac{\partial p'}{\partial x}} \right\rangle_{\mathcal{T}}, \tag{2.1d}$$

$$E^D_{u'^2} = \nu \left\langle -k^2 \hat{u}' \hat{u}'^* + \frac{\partial^2 \hat{u}' \hat{u}'^*}{\partial y^2} \right\rangle_{\mathcal{T}}, \tag{2.1e}$$

$$E^T_{u'^2} = -\left\langle \hat{u}'^* \widehat{\frac{\partial u'_k u'}{\partial x_k}} + \hat{u}' \widehat{\frac{\partial u'_k u'}{\partial x_k}}^* \right\rangle_{\mathcal{T}}, \tag{2.1f}$$

$$E^{\epsilon}_{u'^2} = 2\nu \left\langle \widehat{\frac{\partial u'}{\partial x_k}} \widehat{\frac{\partial u'}{\partial x_k}}^* \right\rangle_{\mathcal{T}} \tag{2.1g}$$

are the spectral densities of $\langle u'u' \rangle$, its rate of production, streamwise pressure transport, diffusion transport and turbulent transport, and dissipation, respectively. Here, $\langle \cdot \rangle_{\mathcal{T}}$ denotes the average over time, $(\cdot)^*$ the complex conjugate, and $\widehat{(\cdot)}$ indicates the Fourier transform in the x and z directions. Also, u_k is the velocity component in the x_k direction where the subscript k is the repeating variable.

For the two-dimensional spectral density of a statistical quantity as a function of k_x and k_z, $E(k_x, k_z)$, the rescaled spectral density in the polar-log coordinates, $E^{\#}$, is used (here, k_x and k_z represent the wavenumbers in the x and z directions, respectively). This form of presentation of the spectral density is introduced to scrutinise the isotropy and the contributions from the $k_x = 0$ or $k_z = 0$ modes (Lee & Moser 2019):

$$E^{\#}(k_x^{\#}, k_z^{\#}) = k^2 E(k_x, k_z)/\xi, \tag{2.2a}$$

where

$$k_x^{\#} = \xi k_x / k, \quad k_z^{\#} = \xi k_z / k, \quad k = \sqrt{k_x^2 + k_z^2}, \tag{2.2b}$$

with $\lambda = 2\pi/k$. Here, k_{ref} is an arbitrary reference wavenumber, and $\xi = \ln(k/k_{ref})$. For inner scaling of the spectra, $k^+_{ref} = 1/50\,000$ and, for outer scaling, $k_{ref}\delta = 1/100$ are

https://doi.org/10.1017/jfm.2025.10844 Published online by Cambridge University Press

chosen. Here, k_{ref} determines the distance from the origin in the polar-log coordinates, and ξ is a logarithmic measure of the distance from the origin. Therefore, k_{ref} should be smaller than the smallest wavenumber of interest, so that ξ is positive. Also, if k_{ref} is too small, it may unnecessarily move the plots away from the origin, making it difficult to see the details of the spectra. In this study, we use $k_{ref} = 1/(50\,000\delta_\nu)$ for inner scaling and $k_{ref} = 1/(100\delta)$ for outer scaling, where δ_ν and δ are the viscous inner and outer length scales, respectively. Note that the integration of $E^{\#}$ over $k_x^{\#}$ and $k_z^{\#}$ remains the same as the integration of E over k_x and k_z.

3. Wall dissipation and turbulent transport

3.1. *Streamwise wall dissipation*

We start by showing the spectral density of the dissipation rate of $\langle u'^2 \rangle$ at the wall, denoted by $E^{\epsilon_w}_{u'^2}$,

$$E^{\epsilon_w}_{u'^2} = E^{\epsilon}_{u'^2}(y=0) = 2\nu \left\langle \widehat{\frac{\partial u'}{\partial y}} \widehat{\frac{\partial \hat{u}'}{\partial y}}^{*} \right\rangle_{\mathcal{T},\, y=0}, \tag{3.1}$$

in figures 2 and 3 for Poiseuille flow. The pre-multiplied spectral density of u'^2 dissipation, $k^2 E^{\epsilon_w}_{u'^2}$ from (2.2*a*) is a function of k_x, k_z, u_τ, ν and δ. In the region close to the wall, $\partial/\partial y \sim O(1/\delta_\nu)$ can be assumed. Also, the energy-containing length scale δ_ν is identical to the Kolmogorov length scale, becoming the smallest possible length scale. We assume a sufficiently high Re_τ, so that the effect of the mean pressure gradient in Poiseuille flow is negligible in this region – for example, the effect of the mean pressure gradient on turbulent production becomes less than 1 % for $y^+ \lesssim 10$ at $Re_\tau \gtrsim 10^3$ (see (3.5)). For $k_x \sim O(1/\delta_\nu)$ and $k_z \sim O(1/\delta_\nu)$, the Buckingham Pi analysis leads the inner-scaled dimensionless pre-multiplied spectral density of $E^{\epsilon_w}_{u'^2}$ to be only a function of k_x^+ and k_z^+, i.e.

$$\frac{k^2 E^{\epsilon_w}_{u'^2}(k_x, k_z)}{u_\tau^2 \delta_\nu^{-2}} = \frac{(k^+)^2 E^{\epsilon_w}_{u'^2}(k_x^+, k_z^+)}{u_\tau^2 \delta_\nu^{-2}} = f(k_x^+, k_z^+). \tag{3.2}$$

Figure 2 confirms this analysis, as the spectral density $E^{\epsilon_w}_{u'^2}$ for $k_x^{\#} \simeq 0$ and $\lambda^+ = 100$ (or $k_z^{\#} = 3.5$) is approximately *Re*-invariant. We note that this is also analogous to the behaviour observed for $\langle u'^2 \rangle$ in previous studies (e.g. Hoyas & Jiménez 2006; Lee & Moser 2015, 2019, see Appendix B).

As discussed in § 1, the length scale of inactive motions is much larger than that of energy-containing motions in the near-wall region. Given that the largest possible wall-parallel length scale is δ, the pre-multiplied spectral density of $E^{\epsilon_w}_{u'^2}$ for $k_x \sim O(1/\delta)$ and $k_z \sim O(1/\delta)$ is written as

$$\frac{k^2 E^{\epsilon_w}_{u'^2}(k_x, k_z)}{u_\tau^2 \delta_\nu^{-2}} = \frac{(k\delta)^2 E^{\epsilon_w}_{u'^2}(k_x\delta, k_z\delta, \delta/\delta_\nu)}{u_\tau^2 \delta_\nu^{-2}} = g(k_x\delta, k_z\delta; Re_\tau), \tag{3.3}$$

where *Re*-dependence appears due to the presence of the two different length scales, δ_ν and δ. A weak *Re*-dependence is confirmed from the outer-scaled spectral intensity in figure 3; although the spectral density around the peak location at $k_x^{\#} \simeq 0$ and $\lambda/\delta = 1$ (or $k_z^{\#} \simeq 2.5$) does not exhibit a visible *Re*-dependence, the region around $k_z \simeq 2k_x$ and $\lambda/\delta = 1$ ($k_x^{\#} \simeq 1.5$ and $k_z^{\#} \simeq 2.5$) shows a gradual weakening in the spectral density with increasing Re_τ.

https://doi.org/10.1017/jfm.2025.10844 Published online by Cambridge University Press

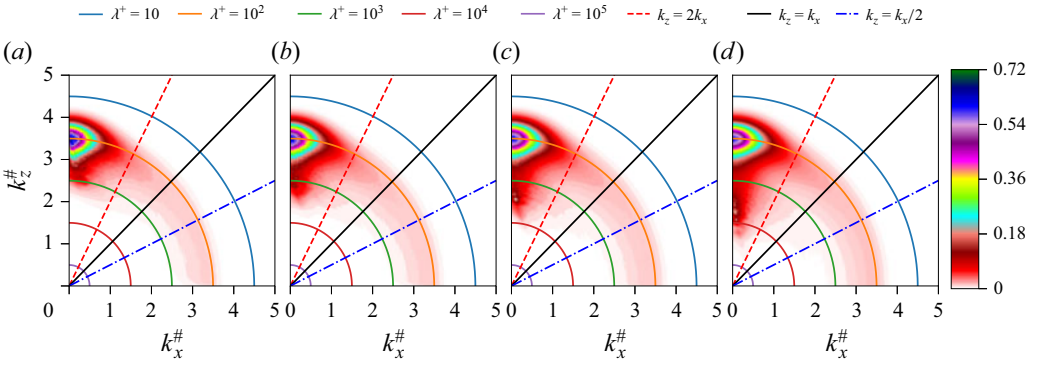

Figure 2. Inner-scale normalised two-dimensional spectral densities in polar-log coordinates of ϵ_w for Poiseuille flows, $k_{ref} = 1/(50\,000\delta_v)$. (*a*) $Re_\tau = 550$ (*b*) $Re_\tau = 1000$ (*c*) $Re_\tau = 2000$ (*d*) $Re_\tau = 5200$. https://www.cambridge.org/S0022112025108446/JFM-Notebooks/files/figure02/Fig02.ipynb.

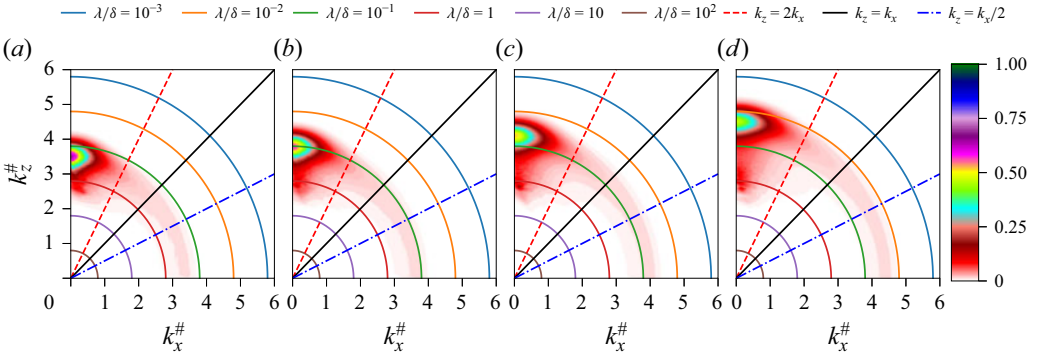

Figure 3. Outer-scale normalised two-dimensional spectral densities in polar-log coordinates of ϵ_w for Poiseuille flows, $k_{ref} = 1/(100\delta)$. (*a*) $Re_\tau = 550$ (*b*) $Re_\tau = 1000$ (*c*) $Re_\tau = 2000$ (*d*) $Re_\tau = 5200$. https://www.cambridge.org/S0022112025108446/JFM-Notebooks/files/figure03/Fig03.ipynb.

Figure 4 shows the rate of streamwise dissipation on the wall, together with its high- and low-pass filtered values using inner- and outer-scaled cutoff wavelengths, $\lambda^+ = 1000$ and $\lambda/\delta = 1$, respectively. We note that for $Re_\tau < 1000$ there is an overlap part between the two filtered quantities. From this viewpoint, these properties are more useful as Re_τ is sufficiently large. The rate of streamwise dissipation on the wall increases with Re, similar to the well-known streamwise turbulence intensity near the wall (figure 4*a*). When the high-pass filter with $\lambda^+ = 1000$ is applied (figure 4*b*), the dissipation rate remains approximately constant in Couette flow at all the Reynolds numbers, consistent with (3.2). In Poiseuille flow, it is seen to asymptotically approach the constant value observed in Couette flow. This difference can be explained with the streamwise mean momentum equation of Poiseuille flow given by

$$\frac{\mathrm{d}U^+}{\mathrm{d}y^+} - \langle u'v' \rangle^+ = \left(1 - \frac{y^+}{Re_\tau}\right), \tag{3.4}$$

where U^+ is the mean streamwise velocity. Here, the Re-dependent last term stems from its mean streamwise pressure gradient. From (3.4), the peak value of the rate of turbulence production is obtained as

$$P^+(y_p^+) = \frac{1}{2}\left(1 - \frac{y_p^+}{Re_\tau}\right), \tag{3.5}$$

https://doi.org/10.1017/jfm.2025.10844 Published online by Cambridge University Press

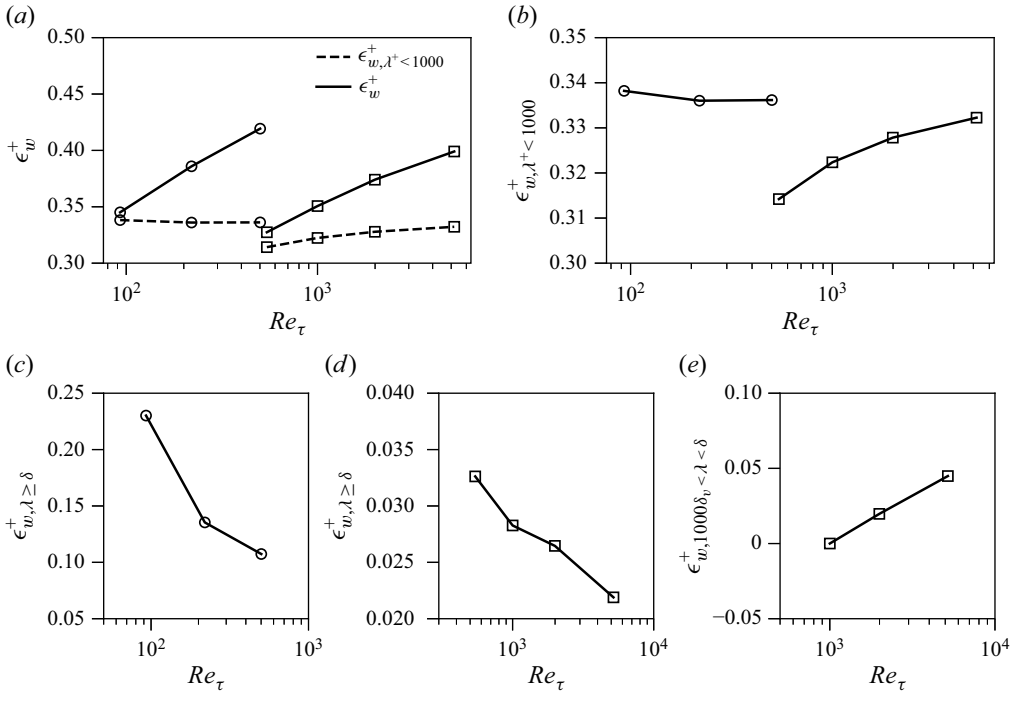

Figure 4. Dissipation rate of $\langle u'^2\rangle^+$ at walls, ϵ_w for Couettte (○) and Poiseuille (□) flows at various Re_τ: (*a*) total and inner-scale-filtered ϵ_w; (*b*) inner-scale-filtered ϵ_w, magnification of (*a*); (*c*) outer-scale-filtered ϵ_w for Couette flow; (*d*) outer-scale-filtered ϵ_w for Poiseuille flow; (*e*) difference between ϵ_w and the sum of inner-scale-filtered ϵ_w and outer-scale-filtered ϵ_w (Poiseuille flow for $Re_\tau > 1000$). https://www.cambridge.org/S0022112025108446/JFM-Notebooks/files/figure04/Fig04.ipynb.

where $P^+ \equiv -2\langle u'v'\rangle^+ \mathrm{d}U^+/\mathrm{d}y^+$ and y_p^+ is its peak wall-normal location near the wall. In Couette flow, $P^+(y_p^+) = 1/2$ for all Reynolds numbers due to the absence of the *Re*-dependent term (i.e. the mean-streamwise-pressure-gradient term) in (3.4). In the near-wall region, turbulence production occurs for $\lambda^+ < 1000$ (Lee & Moser 2019, see also figures 5 and 6 for the filtered budget terms, and figure 11 in the Appendix A for the unfiltered budget terms.) Then, the related dissipation at $\lambda^+ < 1000$ would be directly affected by the production, implying that it would asymptotically reach a constant value as $Re \to \infty$, consistent with figure 4(*b*).

When the streamwise-dissipation rate is low-pass filtered with $\lambda/\delta = 1$ (figure 4*c*,*d*), the remaining part becomes substantially small. However, the small filtered streamwise-dissipation rate decays slowly with *Re*, consistent with the outer-scaled spectral intensity of $E_{u'^2}^{\epsilon_w}$ in figure 3 and the dimensional analysis in (3.3). Given that the dissipation rate for $\lambda^+ < 1000$ is asymptotically constant (figure 4*b*) and that for $\lambda/\delta > 1$ decays with *Re* (figure 4*c*,*d*), the increase in the rate of total streamwise dissipation on the wall with *Re* must be driven primarily by $E_{u'^2}^{\epsilon_w}$ for $1000\delta_\nu < \lambda < \delta$ at high *Re* (figure 4*e*). Note that the range $1000\delta_\nu < \lambda < \delta$ exists only for sufficiently high *Re* (specifically, $Re_\tau > 1000$). For such cases, the contribution to wall dissipation from this intermediate range can be expressed as $\epsilon_{w,\,1000\delta_\nu<\lambda<\delta}^+ = \epsilon_w^+ - \epsilon_{w,\,\lambda^+<1000}^+ - \epsilon_{w,\,\lambda\geqslant\delta}^+$, and the increase of ϵ_w^+ from $Re_\tau = 1000$ to $Re = 5000$ in Poiseuille flow is almost identical to that of $\epsilon_{w,\,1000\delta_\nu<\lambda<\delta}^+$. By definition, this is the length scale associated with the logarithmic layer, supporting the idea of Townsend (1976) that shear stress on the wall contains a fluctuating part associated

https://doi.org/10.1017/jfm.2025.10844 Published online by Cambridge University Press

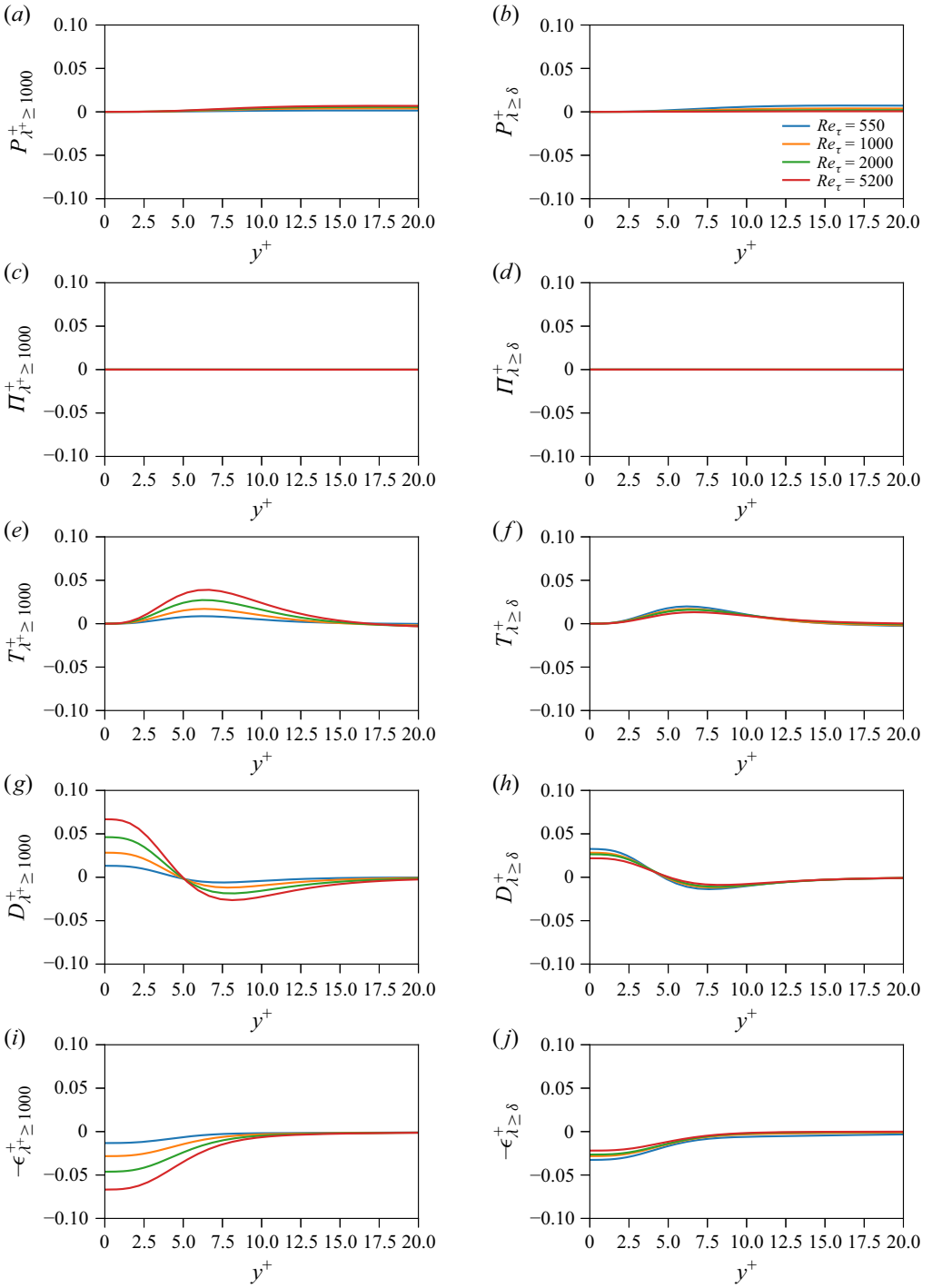

Figure 5. Filtered budget terms near the wall of Poiseuille flows. (*a*,*b*) Production; (*c*,*d*) pressure transport; (*e*,*f*) turbulent transport; (*g*,*h*) viscous transport; (*i*,*j*) dissipation rate. https://www.cambridge.org/S0022112025108446/JFM-Notebooks/files/figure05/Fig05.ipynb.

https://doi.org/10.1017/jfm.2025.10844 Published online by Cambridge University Press

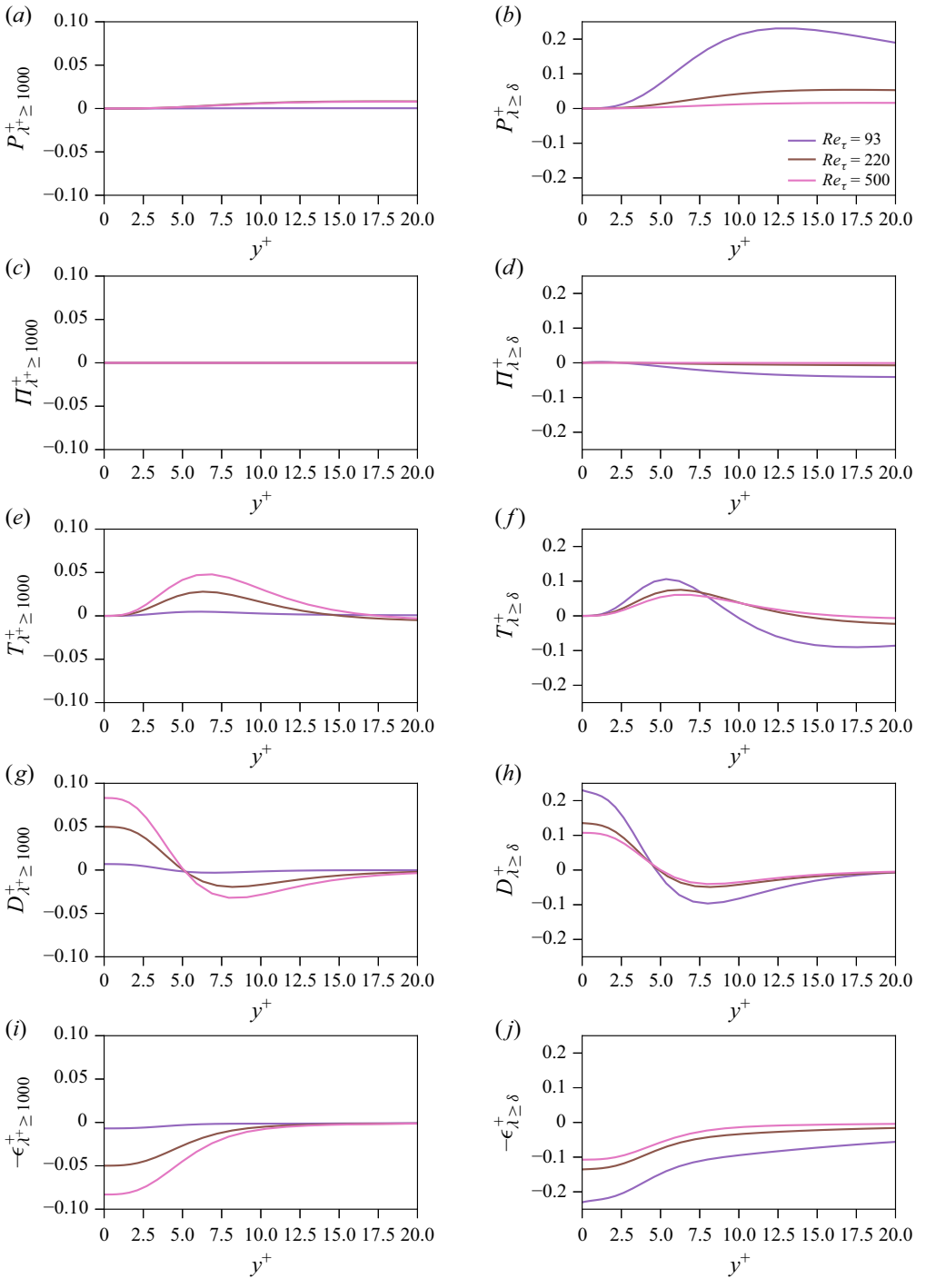

Figure 6. Filtered budget terms near the wall of Couette flows. (*a*,*b*) Production; (*c*,*d*) pressure transport; (*e*,*f*) turbulent transport; (*g*,*h*) viscous transport; (*i*,*j*) dissipation rate. https://www.cambridge.org/S0022112025108446/JFM-Notebooks/files/figure06/Fig06.ipynb.

https://doi.org/10.1017/jfm.2025.10844 Published online by Cambridge University Press

with energy-containing motions in the log and outer regions. We also note that the same behaviour was also observed from the near-wall streamwise velocity variances (Hwang 2024; Pirozzoli 2024, see also Appendix B), consistent with the relation (1.2).

3.2. *Streamwise-spectral-energy budget in near-wall region*

Now, we consider two low-pass filters with the cutoff wavelengths given by $\lambda^+ = 1000$ and $\lambda/\delta = 1$. Their applications to each of the energy-budget terms in (2.1) are shown in figures 5 and 6 for the near-wall region. When $\lambda^+ = 1000$ is considered for the cutoff wavelength (left column of figures 5 and 6), the rates of turbulence production ($P^+_{\lambda^+\geqslant 1000}$) and pressure transport ($\Pi^+_{\lambda^+\geqslant 1000}$) are negligibly small, compared with the other budget terms. Therefore, in the near-wall region (say $y^+ \lesssim 10$), the following energy balance is obtained for the spectral density of streamwise TKE at $\lambda^+ \geqslant 1000$:

$$T^+_{\lambda^+\geqslant 1000} + D^+_{\lambda^+\geqslant 1000} - \epsilon^+_{\lambda^+\geqslant 1000} \simeq 0, \tag{3.6}$$

where T, D and ϵ are the rates of streamwise turbulent transport, viscous diffusion transport and dissipation, respectively. This energy balance is consistent with the concept of 'inactive' motions by Townsend (1976), as these large streamwise motions near the wall do not contain Reynolds shear stress (or turbulence production, equivalently). More importantly, they are driven by turbulent transport, T. Furthermore, given that turbulent transport must vanish at the wall (i.e. $T^+_{\lambda^+\geqslant 1000} = 0$ at $y = 0$), (3.6) becomes

$$D^+_{\lambda^+\geqslant 1000} - \epsilon^+_{\lambda^+\geqslant 1000} = 0 \tag{3.7}$$

at $y = 0$. Since $T^+_{\lambda>1000} > 0$ in the near-wall region, this acts as the source term for non-zero $D^+_{\lambda>1000}$ and $\epsilon^+_{\lambda>1000}$ (see figures 5*c* and 6*c*). We note $\int_\Omega D^+_{\lambda>1000}\mathrm{d}y = 0$, where Ω is the wall-normal domain. Therefore, this suggests that the energy of inactive motions driven by turbulent transport near the wall is transported to the wall by viscous diffusion, which ultimately contributes to dissipation on the wall for $\lambda^+ \geqslant 1000$. The same energy balance is obtained by low-pass filtering with $\lambda/\delta = 1$ as long as Re_τ is sufficiently high (right column of figures 5 and 6). However, for $Re_\tau < 1000$, the outer-scaled filtered wavelength $\lambda = \delta$ becomes $\lambda^+ < 1000$. Therefore, the filtered rate of production ($P^+_{\lambda\geqslant\delta}$) and the pressure transport ($\Pi^+_{\lambda\geqslant\delta}$) are no more negligible due to the contribution from the energy-containing motions in the near-wall region.

In figures 5 and 6, all the terms in (3.6) increase with Re, consistent with the observation in figure 4, where the increase of the streamwise wall dissipation with Re originates primarily from $\epsilon^+_{\lambda^+\geqslant 1000}$. Since the driving term in (3.6) is turbulent transport, we explore its two-dimensional spectral density near the wall further by decomposing into

$$E^{T^\perp}_{u'^2} = -\frac{1}{2}\left\langle \frac{\partial \hat{u}'^* \widehat{u'v'}}{\partial y} + \frac{\partial \hat{u}' \widehat{u'v'}^*}{\partial y} \right\rangle_{\mathcal{T}}, \tag{3.8a}$$

$$E^{T^\parallel}_{u'^2} = E^{T}_{u'^2} - E^{T^\perp}_{u'^2}. \tag{3.8b}$$

Here, $\int_0^{2\delta} E^{T^\perp}_{u'^2}\mathrm{d}y = 0$ for all (k_x, k_z), such that there is no net turbulent transport in the wall-normal direction by $E^{T^\perp}_{u'^2}$. Similarly, $\int\int_0^\infty E^{T^\parallel}_{u'^2}\mathrm{d}k_x\mathrm{d}k_z = 0$ for all y, and there is no net transfer between scales by $E^{T^\parallel}_{u'^2}$ at any given wall-normal distance. Hence, $E^{T^\perp}_{u'^2}$ represents turbulent transport in the wall-normal direction (e.g. energy transport from outer flow;

https://doi.org/10.1017/jfm.2025.10844 Published online by Cambridge University Press

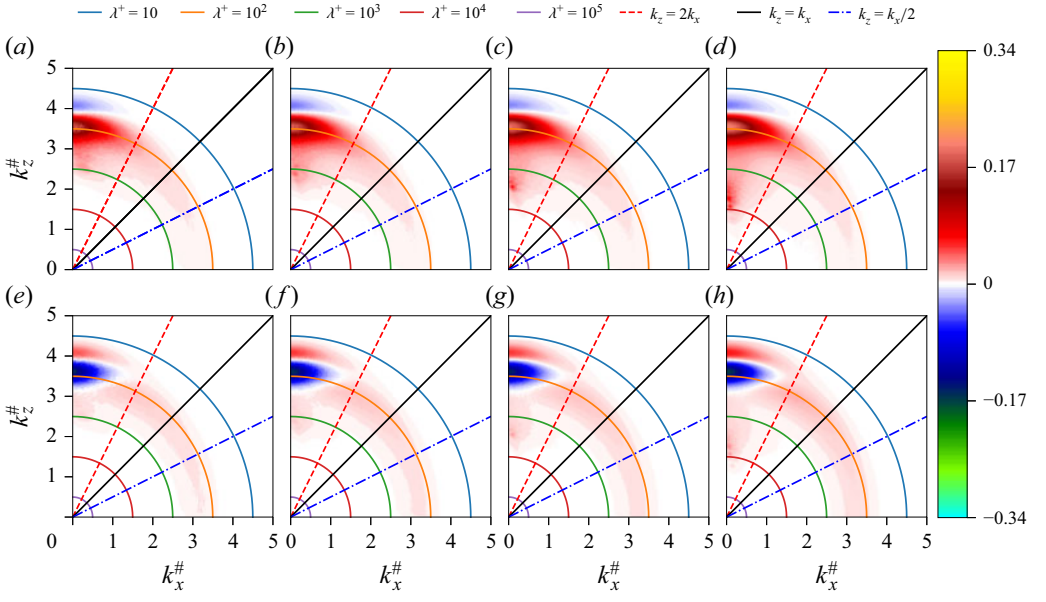

Figure 7. Inner-scale normalised two-dimensional spectral densities of wall-normal transport and inter-scale transfer of $\langle u'^2 \rangle$ in polar-log coordinates, $y^+ = 5$, Poiseuille flows, $k_{ref} = 1/(50\,000\delta_v)$: (*a–d*) wall-normal transport, $T^\perp$; (*e–h*) inter-scale transfer $T^\parallel$. (*a*) $T^\perp_{y^+=5}$, $Re_\tau = 550$ (*b*) $T^\perp_{y^+=5}$, $Re_\tau = 1000$ (*c*) $T^\perp_{y^+=5}$, $Re_\tau = 2000$ (*d*) $T^\perp_{y^+=5}$, $Re_\tau = 5200$ (*e*) $T^\parallel_{y^+=5}$, $Re_\tau = 550$ (*f*) $T^\parallel_{y^+=5}$, $Re_\tau = 1000$ (*g*) $T^\parallel_{y^+=5}$, $Re_\tau = 2000$ (*h*) $T^\parallel_{y^+=5}$, $Re_\tau = 5200$. https://www.cambridge.org/S0022112025108446/JFM-Notebooks/files/figure07/Fig07.ipynb.

Lee & Moser 2019), while $E^{T^\parallel}_{u'^2}$ signifies the inter-scale energy transfer at given wall-normal distances (e.g. inverse energy transfer from small to large scale; Cho *et al.* 2018; Kawata & Alfredsson 2018; Lee & Moser 2019).

Figures 7 and 8 show the inner- and outer-scaled spectral densities of $E^{T^\perp}_{u'^2}$ and $E^{T^\parallel}_{u'^2}$ at $y^+ = 5$ in Poiseuille flow. The positive (red) peak region of $E^{T^\perp}_{u'^2}$ appears at $\lambda^+ \approx 100$ and $k_x^\# \approx 0$ (figure 7*a–d*), indicating the wall-normal energy transport from the elongated streaks (i.e. positive/negative streamwise velocity fluctuations elongated in the streamwise direction) in the buffer layer. The adjacent negative (blue) peak region at $\lambda^+ < 100$ must imply an outward energy transport, given that the spectral density of the streamwise wall dissipation in this region is very small (see figure 2). In the spectra of $E^{T^\parallel}_{u'^2}$ (figure 7*e–h*), a negative (blue) peak region appears at $\lambda^+ \approx 100$ and $k_x^\# \approx 0$, characterising the wall-parallel energy transfer from the energy-containing length scale to the other length scales in the near-wall region. The positive (red) peak region in the same spectra appears at $\lambda^+ < 100$ and $k_x^\# \approx 0$. We note that this peak value is comparable to the magnitude of the negative peak in the $E^{T^\perp}_{u'^2}$ spectra. Given that these two peaks occur on a length scale smaller than $\lambda^+ = 100$ (i.e. classic energy cascade) and involve an outward energy transport, they would statistically represent the near-wall bursting (Kline *et al.* 1967) for the streamwise TKE.

The inner-scaled spectral densities of $E^{T^\perp}_{u'^2}$ associated with the outward energy transport appear to be approximately *Re*-independent (figure 7*a–d*) – given the analysis in § 3.1, even if there exist some variations with *Re*, it is expected that the extent will be as small as $\epsilon^+_{\lambda^+<1000}$ relative to ϵ^+ in figure 4. This is confirmed in figure 9, where the wall-normal

https://doi.org/10.1017/jfm.2025.10844 Published online by Cambridge University Press

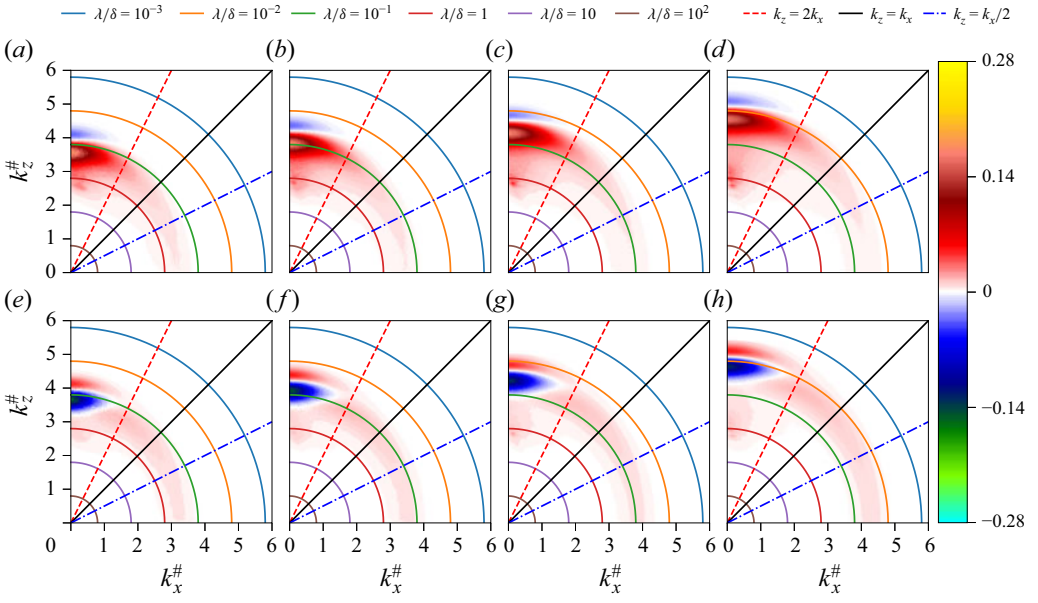

Figure 8. Outer-scale normalised two-dimensional spectral densities of wall-normal transport and inter-scale transfer of $\langle u'^2 \rangle$ in polar-log coordinates, $y^+ = 5$, Poiseuille flows, $k_{ref} = 1/(100\delta)$: (*a–d*) wall-normal transport, $T^{\perp}$; (*e–h*) inter-scale transfer $T^{\parallel}$. (*a*) $T^{\perp}_{y^+=5}, Re_\tau = 550$ (*b*) $T^{\perp}_{y^+=5}, Re_\tau = 1000$ (*c*) $T^{\perp}_{y^+=5}, Re_\tau = 2000$ (*d*) $T^{\perp}_{y^+=5}, Re_\tau = 5200$ (*e*) $T^{\parallel}_{y^+=5}, Re_\tau = 550$ (*f*) $T^{\parallel}_{y^+=5}, Re_\tau = 1000$ (*g*) $T^{\parallel}_{y^+=5}$, $Re_\tau = 2000$ (*h*) $T^{\parallel}_{y^+=5}, Re_\tau = 5200$. https://www.cambridge.org/S0022112025108446/JFM-Notebooks/files/figure08/Fig08.ipynb.

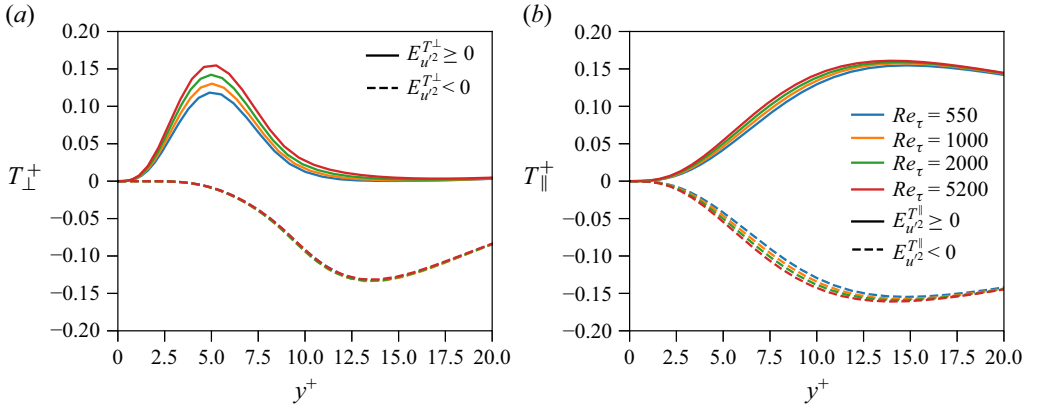

Figure 9. Turbulent transport near the wall of Poiseuille flow, conditioned with the positive and negative part of the corresponding spectra: (*a*) wall-normal transport $T^{\perp}$; (*b*) inter-scale transfer $T^{\parallel}$. https://www.cambridge.org/S0022112025108446/JFM-Notebooks/files/figure09/Fig09.ipynb.

and inter-scale turbulent transport are obtained by conditionally sampling positive and negative parts of the corresponding spectra shown in figure 7. Indeed, the approximate *Re*-independent behaviour of turbulent transport is only observed from $T^{+}_{\perp}$ associated with the loss of TKE (either to the near-wall and outer region; dashed lines in figure 9*a*). Chen & Sreenivasan (2021) recently proposed that the bursting process in the near-wall

https://doi.org/10.1017/jfm.2025.10844 Published online by Cambridge University Press

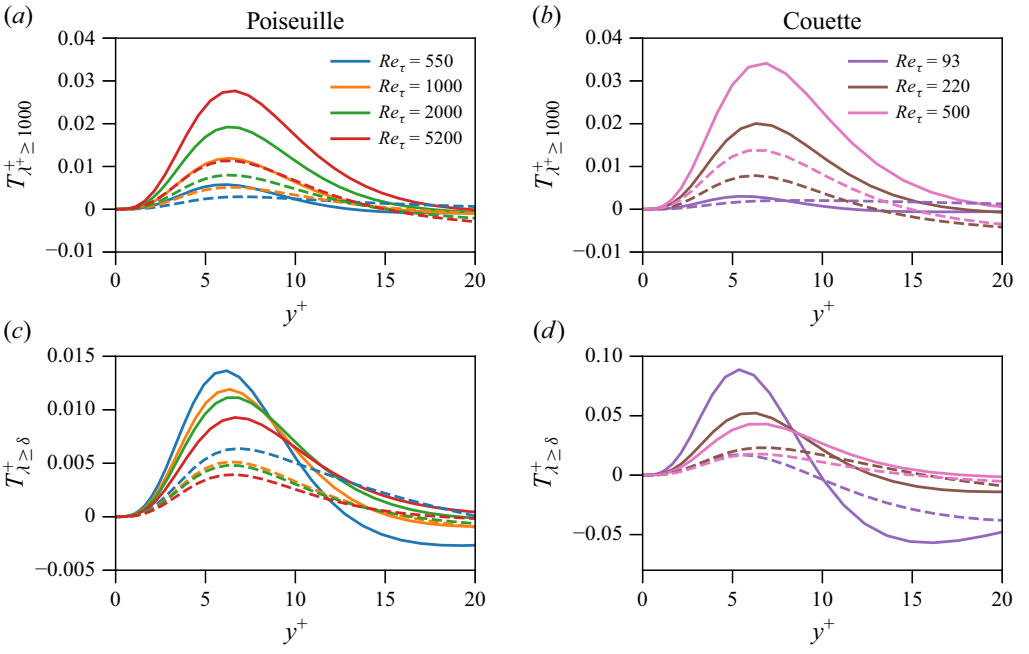

Figure 10. Turbulent wall-normal transport, $T^+_\perp$, and inter-scale transfer, $T^+_\parallel$ of $\langle u'^2\rangle^+$: (——) $T^+_\perp$, (– – –) $T^+_\parallel$. (*a–b*) Inner-scale filtered with $\lambda^+ = 1000$; (*c–d*) outer-scale filtered with $\lambda = \delta$. https://www.cambridge.org/S0022112025108446/JFM-Notebooks/files/figure10/Fig10.ipynb.

region would cause the wall dissipation to vary with Re, and this idea was central in the development of their asymptotic theory for scaling the peak streamwise variances with Re in the near-wall region. However, the bursting-related turbulent transport ($\lambda^+ < 100$ in figure 7 and dashed lines in figure 9*a*) do not support this idea, as they are approximately independent of Re_τ. In fact, the spectra of $E^{T^\perp}_{u'^2}$ and $E^{T^\parallel}_{u'^2}$ depend on Re most strongly for $\lambda^+ > 1000$ like the wall-dissipation spectra in figure 2. This involves the wall-normal energy gain through the wall-normal transport and the inter-scale energy transport, as shown in figure 9 (see later for a further discussion). Furthermore, when the spectra of $E^{T^\perp}_{u'^2}$ and $E^{T^\parallel}_{u'^2}$ are scaled by outer units, their Re-dependent behaviour is qualitatively similar to that of wall dissipation in figure 3 – a small positive peak appears at $\lambda/\delta \approx 1$ and $k^\#_x \approx 0$, and the spectral densities for $\lambda/\delta \approx 1$ and $k_z \approx 2k_x$ slowly decay with Re (figure 8).

To further understand the nature of near-wall turbulent transport, $T_\perp$ and $T_\parallel$ obtained by integrating the related spectra for $\lambda^+ \geqslant 1000$ and $\lambda \geqslant \delta$ are also shown in figure 10. For both Poiseuille and Couette flows, the values of $T_\perp$ and $T_\parallel$ increase with Re_τ, when the spectra of $\lambda^+ \geqslant 1000$ are considered. In contrast, when $\lambda \geqslant \delta$ is considered, the values of $T_\perp$ and $T_\parallel$ decrease with Re_τ. In all the cases considered here, the near-wall turbulent transport is dominated by that of the wall-normal, $T_\perp$, as it is found to be two to three times greater than its inter-scale counterpart, $T_\parallel$. Given that $T_\perp$ is predominantly positive below $y^+ \simeq 10$ (figure 10), this transport originates mainly from $y^+ \geqslant 10$.

4. Discussions

Thus far, we have explored the scaling behaviour of wall-shear-stress fluctuations in both Poiseuille and Couette flows through the rate of wall dissipation, focusing on its

https://doi.org/10.1017/jfm.2025.10844 Published online by Cambridge University Press

streamwise component. A dimensional analysis suggests the inner-scaling nature of the spectra of streamwise wall dissipation for $\lambda \sim O(\delta_\nu)$ and an Re-dependent behaviour for $\lambda \sim O(\delta)$. This was confirmed by DNS data; in particular, the rate of streamwise wall dissipation only accounting for $\lambda^+ \leqslant 1000$ is approximately constant (Couette flow) or reaches the constant asymptotically on increasing Re (Poiseuille flow), while that for $\lambda > \delta$ consistently decays with Re. Subsequently, an energy-budget analysis was performed to relate this observation to the large streamwise motions near the wall ($y^+ \leqslant 10$), which are inactive in the sense that they do not involve Reynold shear stress or turbulence production. It was found that these motions are directly driven by near-wall turbulent transport, which exhibits the same Re-scaling behaviour with the wall dissipation. This was also observed for both the wall-normal and inter-scale turbulent transport at all the Reynolds numbers considered in Couette and Poiseuille flows.

Given that the Re-scaling behaviours of the streamwise wall-dissipation spectra originate from turbulent-transport spectra near the wall, it is useful to investigate the turbulent transport a little further. In the Fourier space, the spectral density of turbulent transport is written as a convolution integral across the entire range of wavenumbers, i.e.

$$E^T_{u'^2}(k_x, k_z) \sim \hat{u}^*(k_x, k_z) \iint_{-\infty}^{\infty} \hat{u}_k(k_x - s_1, k_z - s_2) \frac{\partial \hat{u}(s_1, s_2)}{\partial x_k} \mathrm{d}s_1 \mathrm{d}s_2, \tag{4.1}$$

where s_1 and s_2 are dummy variables. Similar expressions may be written for both $E^{T^\perp}_{u'^2}$ and $E^{T^\parallel}_{u'^2}$, given their definitions in (3.8).

A triadic-wave-interaction form of turbulent transport in (4.1) suggests some possible origins for the Re-dependent behaviours of the large streamwise motions inactive in the near-wall region. First, given their large size relative to the wall-normal location of interest ($y^+ \lesssim 10$), these motions are expected to develop a 'boundary layer' near the wall. In other words, $\hat{u}_j$ for $\lambda^+ > 1000$ near the wall would be a function of Re to satisfy the no-slip boundary condition as in Prandtl's laminar boundary layer (e.g. Schlichting & Gersten 2017). The degree to which each of $\hat{u}_j$ feels the wall would depend on its size (or horizontal wavelengths), since their length scales vary in the range of $O(\delta_\nu) \ll l \lesssim O(\delta)$. For the same reason, the time scale of $\hat{u}_j$ for each k_x and k_z would also matter in characterising the thickness of the boundary layer as in the Stokes second problem (e.g. Schlichting & Gersten 2017). However, perhaps more importantly, the form of (4.1) implies that each of $\hat{u}_j$ is also a consequence of triadic interactions across all wavenumbers. Given that the length scale near the wall varies from $O(\delta_\nu)$ to $O(\delta)$, the most evident Re-dependence of (4.1) would be given in its integration limit, such that

$$E^T_{u'^2}(k_x, k_z) \sim \hat{u}^*(k_x, k_z) \iint_{-cRe_\tau/\delta}^{cRe_\tau/\delta} \hat{u}_j(k_x - s_1, k_z - s_2) \frac{\partial \hat{u}(s_1, s_2)}{\partial x_j} \mathrm{d}s_1 \mathrm{d}s_2, \tag{4.2}$$

where c is a suitable constant that defines the compact support for $\hat{u}_j$ in the wavenumber space. Furthermore, the integrand itself is expected to be a function of Re, as it involves interaction between three pairs of wavenumbers that vary from $O(1/\delta)$ to $O(1/\delta_\nu)$. This suggests that the way $\hat{u}_j$ for $\lambda^+ > 1000$ would feel the existence of the wall would be very different from that of laminar flow due to the triadic wave interactions involved.

The discussion indicates the complexities on the precise origin of the inactive motions near the wall. Previous studies have shown the existence of an inverse energy transfer from small to large λ (Cho *et al.* 2018; Kawata & Alfredsson 2018; Lee & Moser 2019). Given that the wall-normal velocity of these motions is negligible and they are expected to be well correlated below $y^+ \simeq 10$ due to their large size, it is tempting to relate their

https://doi.org/10.1017/jfm.2025.10844 Published online by Cambridge University Press

dynamics to two-dimensional turbulence, where inverse energy cascade is known to be an important turbulent-energy-transport process (e.g. Boffetta & Ecke 2012, for a review). In relation to this, some recent studies have proposed the mechanism of energy transfer from small to large scale (Doohan *et al.* 2021, 2022; Ciola *et al.* 2024). For example, in their numerical simulation where only the two spanwise length scales ($\lambda_z^+ = 100, 200$) were considered, Doohan, Willis & Hwang (2021) showed that the near-wall inverse energy transfer takes place through the subharmonic instability (or transient growth) of the streaks in the buffer layer (Kline *et al.* 1967). An invariant solution of the Navier–Stokes equations underpinning this process was also found (Doohan *et al.* 2022). Taking a step further, Ciola *et al.* (2024) recently proposed that detuned (or sideband) instabilities (general version of the subharmonic instability) of the buffer-layer streaks could be responsible even for the generation of large-scale structures in the logarithmic and outer regions. However, this scenario is not fully compatible with the simulation of Doohan *et al.* (2021), where the time scale of the related inverse energy transfer was found to be much shorter than the typical time scale of energy-containing motions in the log and outer region.

It is also important to note that the inverse transfer of energy from small to large scales is not the only important turbulent-transport process in the near-wall region (Lee & Moser 2019). Indeed, the wall-normal turbulent transport below $y^+ \simeq 10$ has been shown to be consistently greater than its inter-scale counterpart (figure 10). Furthermore, the wall-normal turbulent transport at $\lambda^+ > 1000$ is mostly positive for $y^+ \lesssim 10$ and monotonically decays as $y \to 0$ (figure 7). This indicates that a great part of the near-wall turbulence at such wavelengths is a consequence of energy transfer towards the wall from above $y^+ \approx 10$. This observation is also consistent with recent observations on the direct transfer of energy and moment from the outer to the near-wall region (Deshpande *et al.* 2024; Yin *et al.* 2024). Here, it is worth recalling again that the large inactive motions near the wall contain very little wall-normal velocity. This implies that this energy and momentum transfer towards the wall is only possible through nonlinear interactions with the 'active' near-wall energy-containing motions at $\lambda^+ < 1000$ (quasi-streamwise vortices, in particular), as these are the only motions containing the wall-normal velocity near the wall. This feature highlights that the scale interactions depicted by (4.1) in turbulent energy transport near the wall are presumably very different from those of two-dimensional turbulence.

Supplementary material. Computational Notebook files are available as supplementary material at https://doi.org/10.1017/jfm.2025.10844 and online at https://www.cambridge.org/S0022112025108446/JFM-Notebooks.

Funding. This research used resources of the Argonne Leadership Computing Facility, a US Department of Energy (DOE) Office of Science user facility at Argonne National Laboratory and is based on research supported by the US DOE Office of Science-Advanced Scientific Computing Research Program, under contract no. DE-AC02-06CH11357. Y.H. gratefully acknowledges financial support from the European Office of Aerospace Research and Development (FA8655-23-1-7023; Program Manager: Dr D. Smith).

Declaration of interests. The authors report no conflict of interest.

Data availability statement. Part of the data that support the findings of this study are openly available at https://lee.me.uh.edu.

Appendix A. Budget terms in near-wall regions

The budget terms of $\langle u'^2 \rangle^+$ are shown in figure 11 for all Re_τ considered in both Poiseuille and Couette flow.

https://doi.org/10.1017/jfm.2025.10844 Published online by Cambridge University Press

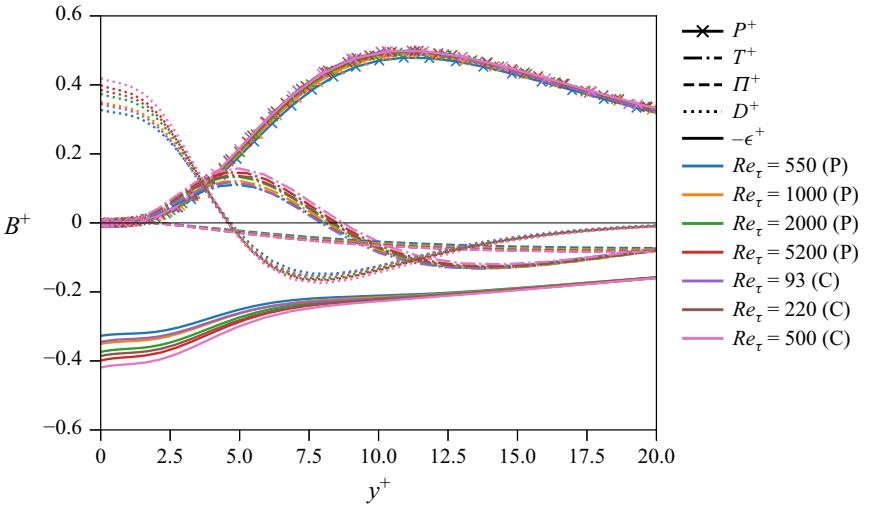

Figure 11. Budget terms, B^+, of $\langle u'^2\rangle^+$ in near-wall regions: P - Poiseuille, C - Couette. https://www.cambridge.org/S0022112025108446/JFM-Notebooks/files/figure11/Fig11.ipynb.

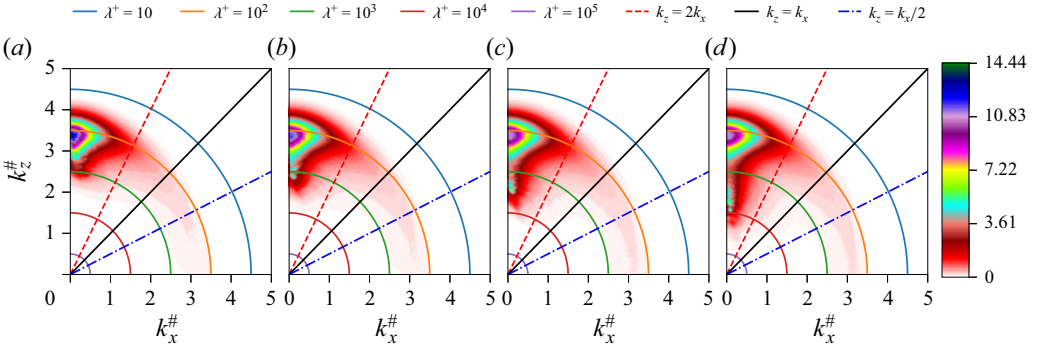

Figure 12. Two-dimensional spectral densities of Poiseuille flows in polar-log coordinates of u'^2 at $y^+ = 15$, $k_{ref} = 1/(50\,000\delta_v)$. (*a*) $Re_\tau = 550$ (*b*) $Re_\tau = 1000$ (*c*) $Re_\tau = 2000$ (*d*) $Re_\tau = 5200$. https://www.cambridge.org/S0022112025108446/JFM-Notebooks/files/figure12/Fig12.ipynb.

Appendix B. Spectra and filtering of streamwise velocity fluctuations

Figures 12 and 13 show the two-dimensional spectral densities of $\langle u'^2\rangle$, denoted by $E^\#_{u'^2}$, in the polar-log coordinate for Poiseuille flow. Overall, the changes in the spectral densities of $E^\#_{u'^2}$ with Re_τ are very similar to those of ϵ_w reported in figures 2 and 3: the spectral density around the peak location at $k_x^\# \simeq 0$ and $\lambda/\delta = 1$ (or $k_z^\# \simeq 2.5$) does not exhibit a visible Re-dependence, but the region around $k_z \simeq 2k_x$ and $\lambda/\delta = 1$ ($k_x^\# \simeq 1.5$ and $k_z^\# \simeq 2.5$) gradually weakens with increasing Re_τ. The spectral densities are also seen to exhibit a good scale separation at a normalised wavelength, $\lambda^+ = 1000$ (see also Lee & Moser 2018, 2019).

By applying a high-pass filter with the cutoff threshold $\lambda^+ = 1000$ to the $\langle u'^2\rangle$ data, a universal behaviour in the small scale is observed like wall-shear-stress fluctuations in both Poiseuille and Couette flows (figure 14*a*,*b*), which persists up to $y^+ \approx 70$ for various values of Re. We note that the identified filtering threshold would be applicable to other canonical wall-bounded turbulent flows, such as pipe (Ahn *et al.* 2015; Pirozzoli *et al.*

https://doi.org/10.1017/jfm.2025.10844 Published online by Cambridge University Press

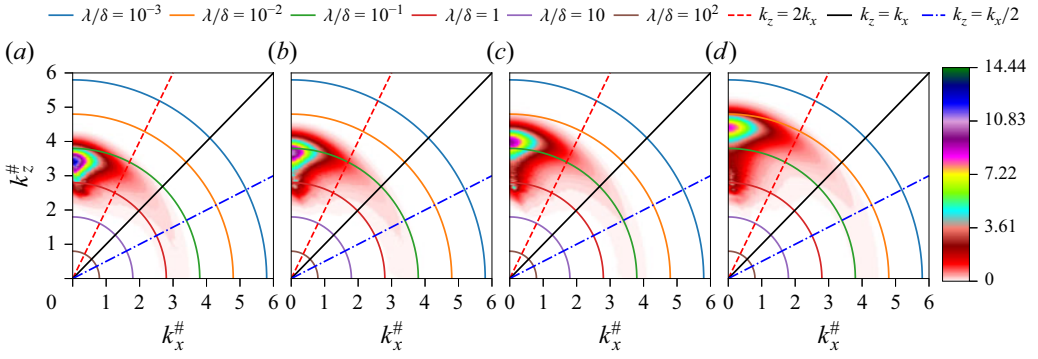

Figure 13. Two-dimensional spectral densities of Poiseuille flows in polar-log coordinates of u'^2 at $y^+ = 15$, $k_{ref} = 1/(100\delta)$. (*a*) $Re_\tau = 550$ (*b*) $Re_\tau = 1000$ (*c*) $Re_\tau = 2000$ (*d*) $Re_\tau = 5200$. https://www.cambridge.org/S0022112025108446/JFM-Notebooks/files/figure13/Fig13.ipynb.

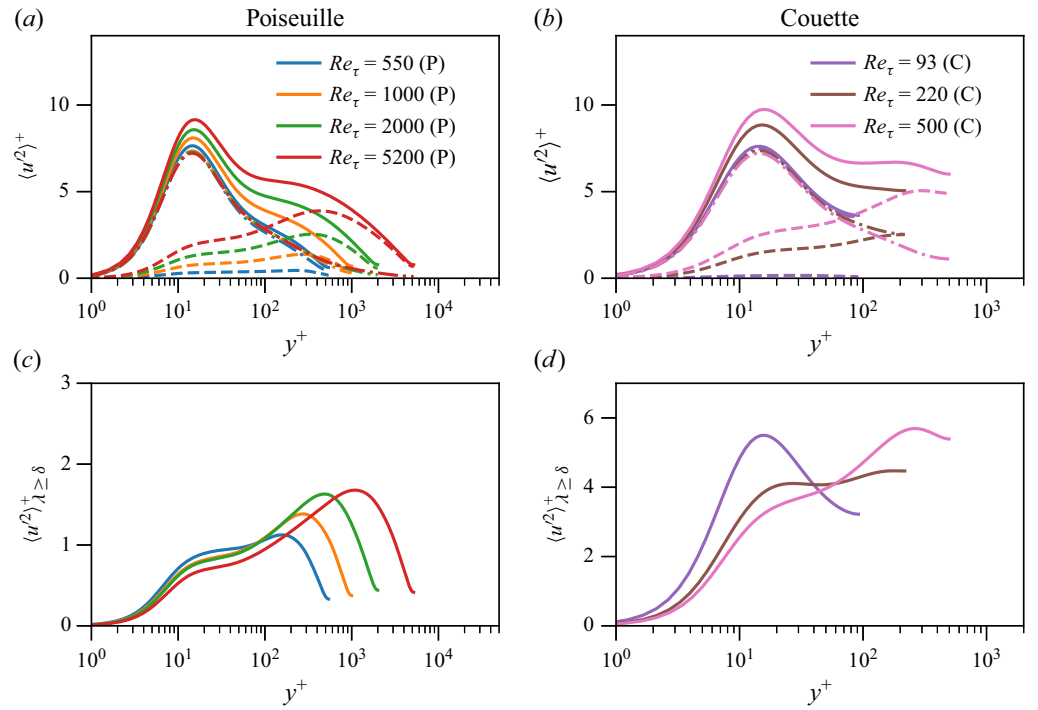

Figure 14. Streamwise velocity variances: (*a*,*b*) (——) $\langle u'^2\rangle^+$, (– · –) $\langle u'^2\rangle^+_{\lambda^+<1000}$, (– – –), $\langle u'^2\rangle^+_{\lambda^+\geqslant 1000}$; (*c*,*d*) (——), $\langle u'^2\rangle^+_{\lambda\geq\delta}$. https://www.cambridge.org/S0022112025108446/JFM-Notebooks/files/figure14/Fig14.ipynb.

2021; Yao *et al.* 2023) and boundary-layer flows (Sillero, Jiménez & Moser 2013; Samie *et al.* 2018), with the expectation of producing the same turbulence statistics on the small scale. Finally, when a low-pass filter with the cutoff threshold $\lambda = \delta$, $\langle u'^2\rangle$ near the wall ($y^+ \lesssim 10$) slowly decays with Re_τ (figure 14*c*,*d*), consistent with the behaviour observed in the filtered wall dissipation, ϵ_w (figure 4*c*,*d*).

https://doi.org/10.1017/jfm.2025.10844 Published online by Cambridge University Press

References

Ahn, J., Lee, J. H., Lee, J., Kang, J.-h. & Sung, H.J. 2015 Direct numerical simulation of a 30R long turbulent pipe flow at $Re_\tau = 3008$. *Phys. Fluids* **27**, 065110.

Boffetta, G. & Ecke, R.E. 2012 Two-dimensional turbulence. *Annu. Rev. Fluid Mech.* **44**, 427–451.

Bradshaw, P. 1967 'Inactive' motion and pressure fluctuations in turbulent boundary layers. *J. Fluid Mech.* **30** (2), 241–258.

Chen, X. & Sreenivasan, K.R. 2021 Reynolds number scaling of the peak turbulence intensity in wall flows. *J. Fluid Mech.* **908**, R3.

Chen, X. & Sreenivasan, K.R. 2022 Law of bounded dissipation and its consequences in turbulent wall flows. *J. Fluid Mech.* **933**, A20.

Cho, M., Hwang, Y. & Choi, H. 2018 Scale interactions and spectral energy transfer in turbulent channel flow. *J. Fluid Mech.* **854**, 474–504.

Ciola, N., De Palma, P., Robinet, J.-C. & Cherubini, S. 2024 Large-scale coherent structures in turbulent channel flow: a detuned instability of wall streaks. *J. Fluid Mech.* **997**, A18.

De Graaff, D.B. & Eaton, J.K. 2000 Reynolds-number scaling of the flat-plate turbulent boundary layer. *J. Fluid Mech.* **422**, 319–346.

Deshpande, R., Monty, J.P. & Marusic, I. 2020 Active and inactive components of the streamwise velocity in wall-bounded turbulence. *J. Fluid Mech.* **914**.

Deshpande, R., Vinuesa, R., Klewicki, J. & Marusic, I. 2024 Active and inactive contributions to the wall pressure and wall-shear stress in turbulent boundary layers. *J. Fluid Mech.* **996**, A12.

Doohan, P., Bengana, Y., Yang, Q., Willis, A.P. & Hwang, Y. 2022 The state space and travelling-wave solutions in two-scale wall-bounded turbulence. *J. Fluid Mech.* **947**, A41.

Doohan, P., Willis, A.P. & Hwang, Y. 2021 Minimal multi-scale dynamics of near-wall turbulence. *J. Fluid Mech.* **913**, A8.

Hoyas, S. & Jiménez, J. 2006 Scaling of the velocity fluctuations in turbulent channels up to $Re_\tau = 2003$. *Phys. Fluids* **18**, 011702.

Hoyas, S. & Oberlack, M. 2024 Turbulent Couette flow up to $re_a u = 2000$. *J. Fluid Mech.* **987**, R9.

Hultmark, M., Vallikivi, M., Bailey, S.C.C. & Smits, A.J. 2012 Turbulent pipe flow at extreme Reynolds numbers. *Phys. Rev. Lett.* **108**, 094501.

Hutchins, N. & Marusic, I. 2007 Evidence of very long meandering features in the logarithmic region of turbulent boundary layers. *J. Fluid Mech.* **579**, 1–28.

Hwang, Y. 2015 Statistical structure of self-sustaining attached eddies in turbulent channel flow. *J. Fluid Mech.* **767**, 254–289.

Hwang, Y. 2016 Mesolayer of attached eddies in turbulent channel flow. *Phys. Rev. Fluids* **1** (6), 064401.

Hwang, Y. 2024 Near-wall streamwise turbulence intensity as $Re_\tau \to \infty$. *Phys. Rev. Fluids* **9**, 044961.

Hwang, Y. & Lee, M. 2020 The mean logarithm emerges with self-similar energy balance. *J. Fluid Mech.* **903**, R6.

Jeong, J., Benney, F., Schoppa, W. & Kim, J. 1997 Coherent structures near the wall in a turbulent channel flow. *J. Fluid Mech.* **332**, 185–214.

Ji, H., Burin, M., Schartman, E. & Goodman, J. 2006 Hydrodynamic turbulence cannot transport angular momentum effectively in astrophysical disks. *Nature* **444**, 343–346.

Jimenez, J. 2024 The near-wall layer at high $Re_a u$ is part of the outer flow. *J. Fluid Mech.*

Kawata, T. & Alfredsson, P.H. 2018 Inverse interscale transport of the Reynolds shear stress in plane Couette turbulence. *Phys. Rev. Lett.* **120**, 244501.

Kline, S.J., Reynolds, W.C., Schraub, F.A. & Runstadler, P.W. 1967 The structure of turbulent boundary layers. *J. Fluid Mech.* **30**, 741–773.

Lee, M., Malaya, N. & Moser, R.D. 2013 Petascale direct numerical simulation of turbulent channel flow on up to 786K cores. In Proceedings of the International Conference on High Performance Computing, Networking, Storage and Analysis, pp. 1–11. ACM Press.

Lee, M. & Moser, R.D. 2015 Direct numerical simulation of turbulent channel flow up to $Re_\tau \approx 5200$. *J. Fluid Mech.* **774**, 395–415.

Lee, M. & Moser, R.D. 2018 Extreme-scale motions in turbulent plane Couette flows. *J. Fluid Mech.* **842**, 128–145.

Lee, M. & Moser, R.D. 2019 Spectral analysis of the budget equation in turbulent channel flows at high Reynolds number. *J. Fluid Mech.* **860**, 886–938.

Marston, J.B., Chini, G.P. & Tobias, S.M. 2016 Generalized quasilinear approximation: application to zonal jets. *Phys. Rev. Lett.* **116**, 214501.

Marusic, I. & Kunkel, G.J. 2003 Streamwise turbulent intensity formulation for flat-flate boundary layers. *Phys. Fluids* **15** (8), 2461.

https://doi.org/10.1017/jfm.2025.10844 Published online by Cambridge University Press

MARUSIC, I., MATHIS, R. & HUTCHINS, N. 2010*a* Predictive model for wall-bounded turbulent flow. *Science* **329**, 193–196.

MARUSIC, I., MCKEON, B.J., MONKEWITZ, P.A., NAGIB, H.M., SMITS, A.J. & SREENIVASAN, K.R. 2010*b* Wall-bounded turbulent flows at high Reynolds numbers: recent advances and key issues. *Phys. Fluids* **22**, 065103.

MARUSIC, I. & MONTY, J.P. 2019 Attached eddy model of wall turbulence. *Annu. Rev. Fluid Mech.* **51**, 49–74.

MATHIS, R., HUTCHINS, N. & MARUSIC, I. 2009 Large-scale amplitude modulation of the small-scale structures in turbulent boundary layers. *J. Fluid Mech.* **628**, 311–337.

MATHIS, R., MARUSIC, I., CHERNYSHENKO, S.I. & HUTCHINS, N. 2013 Estimating wall-shear-stress fluctuations given an outer region input. *J. Fluid Mech.* **715**, 163–180.

MCKEON, B.J. 2017 The engine behind (wall) turbulence: perspectives on scale interactions. *J. Fluid Mech.* **817**, P1.

MONKEWITZ, P.A. 2022 Asymptotics of streamwise Reynolds stress in wall turbulence. *J. Fluid Mech.* **931**, A18.

NICKELS, T., MARUSIC, I., HAFEZ, S. & CHONG, M.S. 2005 Evidence of the k1−1 law in a high-Reynolds-number turbulent boundary layer. *Phys. Rev. Lett.* **95**, 074501.

PERRY, A.E., HENBEST, S. & CHONG, M.S. 1986 A theoretical and experimental study of wall turbulence. *J. Fluid Mech.* **165**, 163–199.

PIROZZOLI, S. 2024 On the streamwise velocity variance in the near-wall region of turbulent flows. *J. Fluid Mech.* **989**, A5.

PIROZZOLI, S., ROMERO, J., FATICA, M., VERZICCO, R. & ORLANDI, P. 2021 One-point statistics for turbulent pipe flow up to $Re_{a}uapprox6000$. *J. Fluid Mech.* **926**, A28.

SAMIE, M., MARUSIC, I., HUTCHINS, N., FU, M.K., FAN, Y., HULTMARK, M. & SMITS, A.J. 2018 Fully resolved measurements of turbulent boundary layer flows up to $Re_{\tau} = 20000$. *J. Fluid Mech.* **851**, 391–415.

SCARSELLI, D., LOPEZ, J.M., VARSHNEY, A. & HOF, B. 2023 Turbulence suppression by cardiac-cycle inspired driving of pipe flow. *Nature* **621** (7977), 71–74.

SCHLATTER, P. & ÖRLÜ, R. 2010 Assessment of direct numerical simulation data of turbulent boundary layers. *J. Fluid Mech.* **659**, 116–126.

SCHLICHTING, H. & GERSTEN, K. 2017 *Boundary-Layer Theory*, 9th edn. Springer.

SILLERO, J.A., JIMÉNEZ, J. & MOSER, R.D. 2013 One-point statistics for turbulent wall-bounded flows at Reynolds numbers up to $\delta^{+} \approx 2000$. *Phys. Fluids* **25**, 105102.

SMITS, A.J., HULTMARK, M., LEE, M., PIROZZOLI, S. & WU, X. 2021 Reynolds stress scaling in the near-wall region of wall-bounded flows. *J. Fluid Mech.* **926**, A31.

TOWNSEND, A.A. 1976 *The Structure of Turbulent Shear Flow*, 2nd edn. Cambridge University Press.

YAO, J., REZAEIRAVESH, S., SCHLATTER, P. & HUSSAIN, F. 2023 Direct numerical simulations of turbulent pipe flow up to $Re_{a}uapprox5200$. *J. Fluid Mech.* **956**, A18.

YIN, L., HWANG, Y. & VASSILICOS, J.C. 2024 Dynamics of turbulent energy and dissipation in channel flow. *J. Fluid Mech.* **996**, A12.

https://doi.org/10.1017/jfm.2025.10844 Published online by Cambridge University Press